Progress in Flight Physics **9** (2017) 435-450
DOI: 10.1051/eucass/201709435

EVOLUTION OF A WAVE PACKET TO TURBULENT SPOT IN A BOUNDARY LAYER AT HIGH SPEEDS

P. A. Polivanov, Yu. V. Gromiko, D. A. Bountin, A. A. Sidorenko, and A. A. Maslov

Khristianovich Institute of Theoretical and Applied Mechanics
Siberian Branch of the Russian Academy of Sciences
4/1 Institutskaya Str., Novosibirsk 630090, Russia

Hypersonic boundary layer stability and transition were studied experimentally for the test case of 7 degree half-angle cone with various nose bluntness. The experiments were performed for M = 6. Wall pressure pulsations were recorded synchronously with the high-speed schlieren. The combined data processing algorithm for coupling of unsteady pressure sensors with high-speed schlieren images was proposed. Analysis of the wall pressure pulsations evolution reveals that the turbulent spot may arise in different ways. It was found that for the blunted model, the role of the second mode in origination of the turbulent spot is more evident.

1 INTRODUCTION

Nowadays, the most popular experimental method to study the nature of laminar–turbulent transition in short-duration wind tunnels is using of surface mounted unsteady sensors. An analysis and interpretation of the measured pressure pulsations is a complicated problem. The level of pressure fluctuations on the wall strongly depends on the type of instability mode and flow parameters. For example, the waves of the second mode which is of acoustic nature can produce stronger pressure pulsations on the wall than the turbulent structures. Since the spectral characteristics of the nonlinear stage of transition and turbulent regime are poorly investigated, these data do not clearly define the flow regime. The schlieren technique can be used to improve understanding of the laminar–turbulent transition. In paper [1], the increase of the boundary layer thickness was used to recognize the turbulent spots. In paper [2], cross-correlation image analysis was used to find periodic structures in the boundary

layer. In this study, the measurements of unsteady wall pressure supplemented with schlieren technique allowed to find characteristic spectra of pressure pulsations depending on the evolution stage of the wave packet and flow parameters.

2 WIND TUNNEL EXPERIMENTS

2.1 Experimental Setup

The supersonic wind tunnel "Tranzit-M" is a short duration aerodynamic facility with range of Mach number M = 4–8 and high values of Reynolds number [3]. The scheme of the wind tunnel is presented in Fig. 1. Initially, the air is accumulated in the first prechamber and volumes of the ohmic heaters, where after heating it acquires high temperature and pressure. After opening of the high-speed valve, the gas is throttled into the second prechamber and afterwards, it flows into the test section through the contoured nozzle. Runtime of the wind tunnel is limited by the volume of the vacuum tank (6.5 m^3) and is approximately equal to 110–200 ms for M = 6. The wind tunnel is equipped with pressure and temperature sensors in the first and second prechambers. The diameter of the contoured nozzle is 300 mm.

The experiments were carried out at M = 6, stagnation temperature T_0 = 370 K, and stagnation pressure P_0 = 3.8–12 bar. The Reynolds number was varied in a range of $\mathrm{Re}_1 = (4 \ldots 20) \cdot 10^6$ m^{-1}. Figure 2 shows variation of the parameters P_0 and T_0 measured in the second prechamber during a run of the wind tunnel. It can be seen that after the opening of the fast valve, there is a graduate change of stagnation parameters. For each run, the data analysis

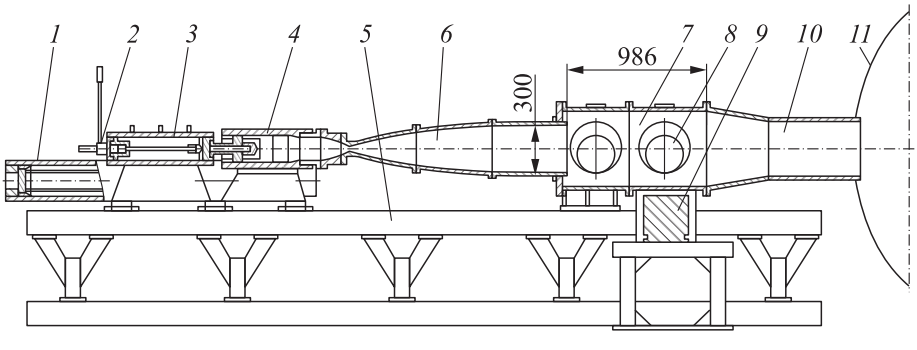

Figure 1 Wind tunnel "Tranzit-M:" *1* — ohmic heater; *2* — high-speed valve; *3* — first prechamber; *4* — second prechamber; *5* — frame; *6* — contoured nozzle; *7* — test section; *8* — optical windows; *9* — isolated model base; *10* — diffuser; and *11* — vacuum tank. Dimensions are in millimeters

was performed for a time window where Re_1 variation was within 5%. The corresponding time window is shown in Fig. 2. The duration of the window was varied from 90 to 200 ms depending on the initial flow parameters. To obtain P_0 and T_0, the pressure and temperature data were averaged within the window. Investigation of free stream noise of the tunnel revealed that the noise level was about 3% [4].

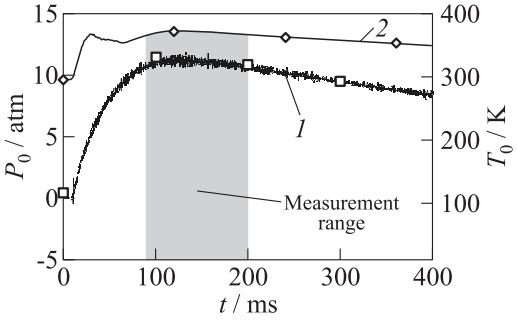

Figure 2 Stagnation pressure (*1*) and temperature (*2*) of the flow during a run

The model is a 7 degree half-angle sharp cone of $L = 0.45$ m length. The model has changeable nose-tips with bluntness radii $R_n = 0.07$ (sharp nose-tip), 0.75, 1.5, and 2 mm. The cone was tested at zero angle of attack. The model is equipped by five pressure sensors PCB 132A31 to measure pulsations of a surface pressure. The longitudinal coordinates of the sensors are as follows: $X = 111.2$, 218.6, 283.6, 348.6, and 413.6 mm. Pressure sensors were used with a signal converter PCB Piezotronocs 482C05. The data were recorded by means of ADC (analog-to-digital converter) L-card E20-10 with sampling frequency 2 MHz. Intrinsic noise of pressure sensors were measured before each experiment and taken into account in processing of data.

Schlieren visualization was performed to determine the local boundary layer thickness and finding periodic structures within the boundary layer in the region of the laminar–turbulent transition. High-speed camera Phantom 310m was used with frame rate 23.5 kHz and exposure time 2 μs. The light source was a xenon lamp (35 W).

The video data processing was performed in two ways. The first technique was used to obtain the local boundary layer thickness. To do this, the time averaged image corresponding to "no flow" condition was subtracted from all images. After that, an image was processed with erosion function with window of 5×3 pixel. The resulting image was used to calculate vertical gradient of intensity and the boundary layer edge was defined as a curve of minimum of the intensity gradient. An example of the image processing is presented in Fig. 3*a*. Curve *1* is the boundary layer edge.

The light source applied for schlieren visualization had some minor oscillations of intensity; therefore, another method was necessary to develop to obtain the flow pulsations from the schlieren image. To eliminate the low frequency oscillations, an image was subtracted by the average image calculated basing on 40 neighboring images. An example of the resulting image can be found in

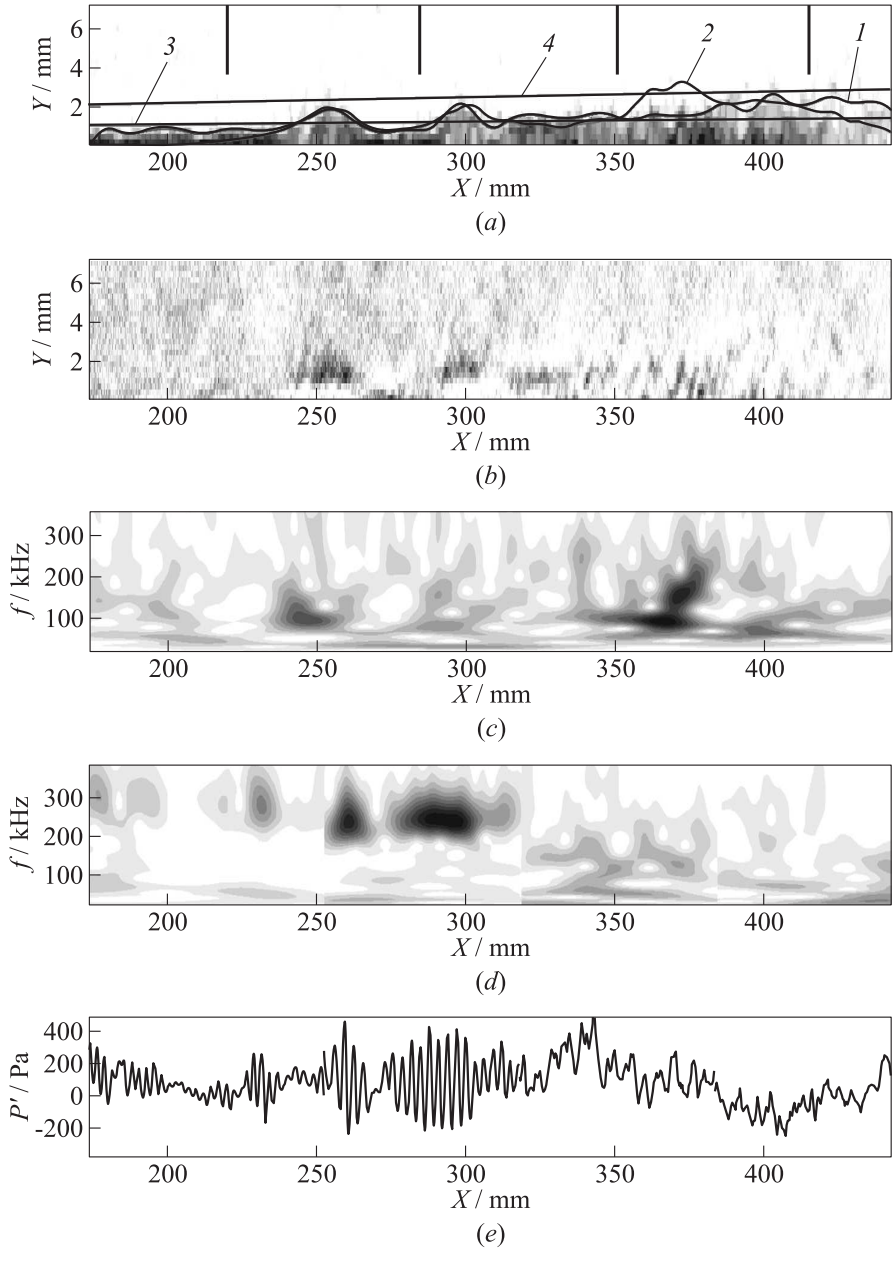

Figure 3 The data processing of schlieren image at $t_{\text{spot}} = 0.043$ ms, $\text{Re}_1 = 8.5 \cdot 10^6$ m^{-1}, and $R_n = 0.07$ mm

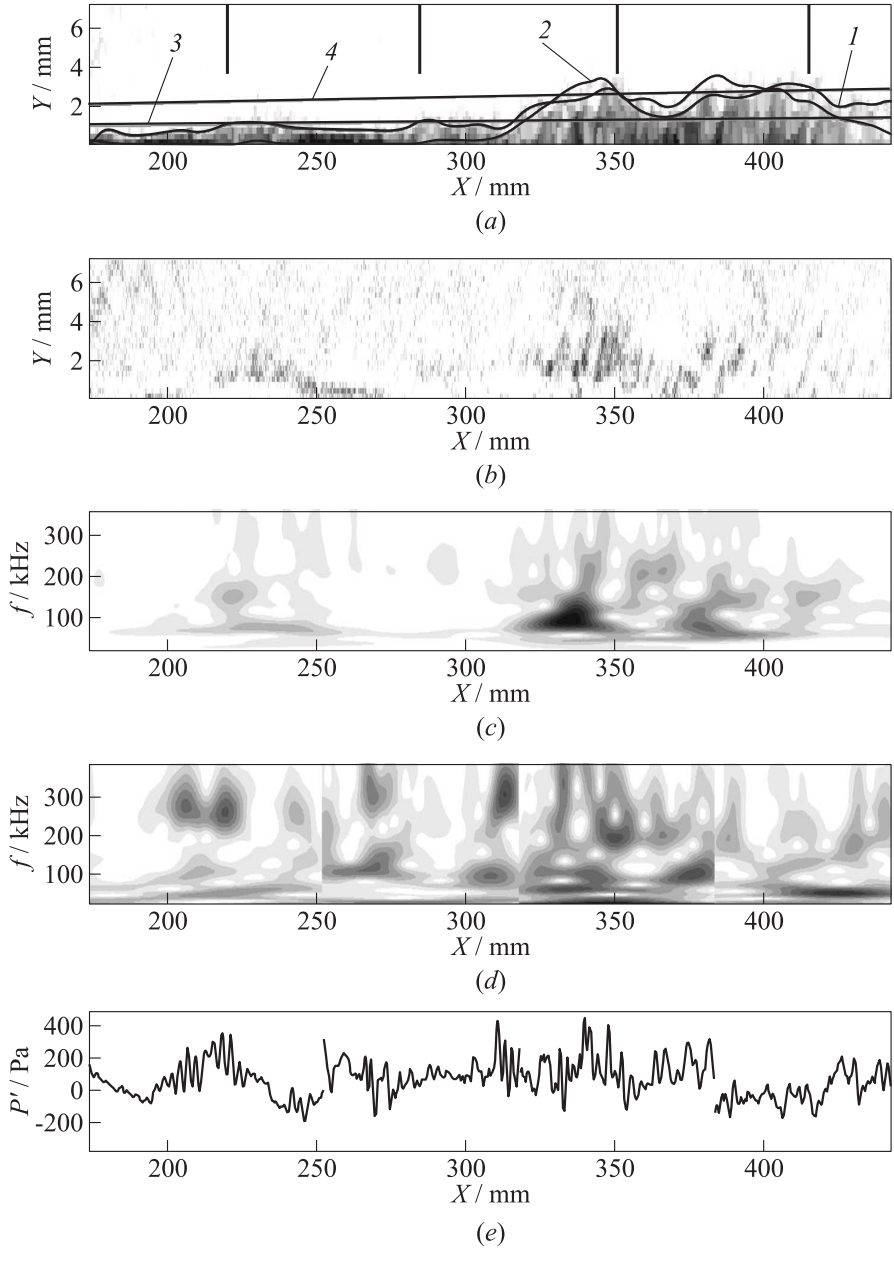

Figure 4 The data processing of schlieren image at $t_{\text{spot}} = 0.128$ ms, $\text{Re}_1 = 8.5 \cdot 10^6$ m^{-1}, and $R_n = 0.07$ mm

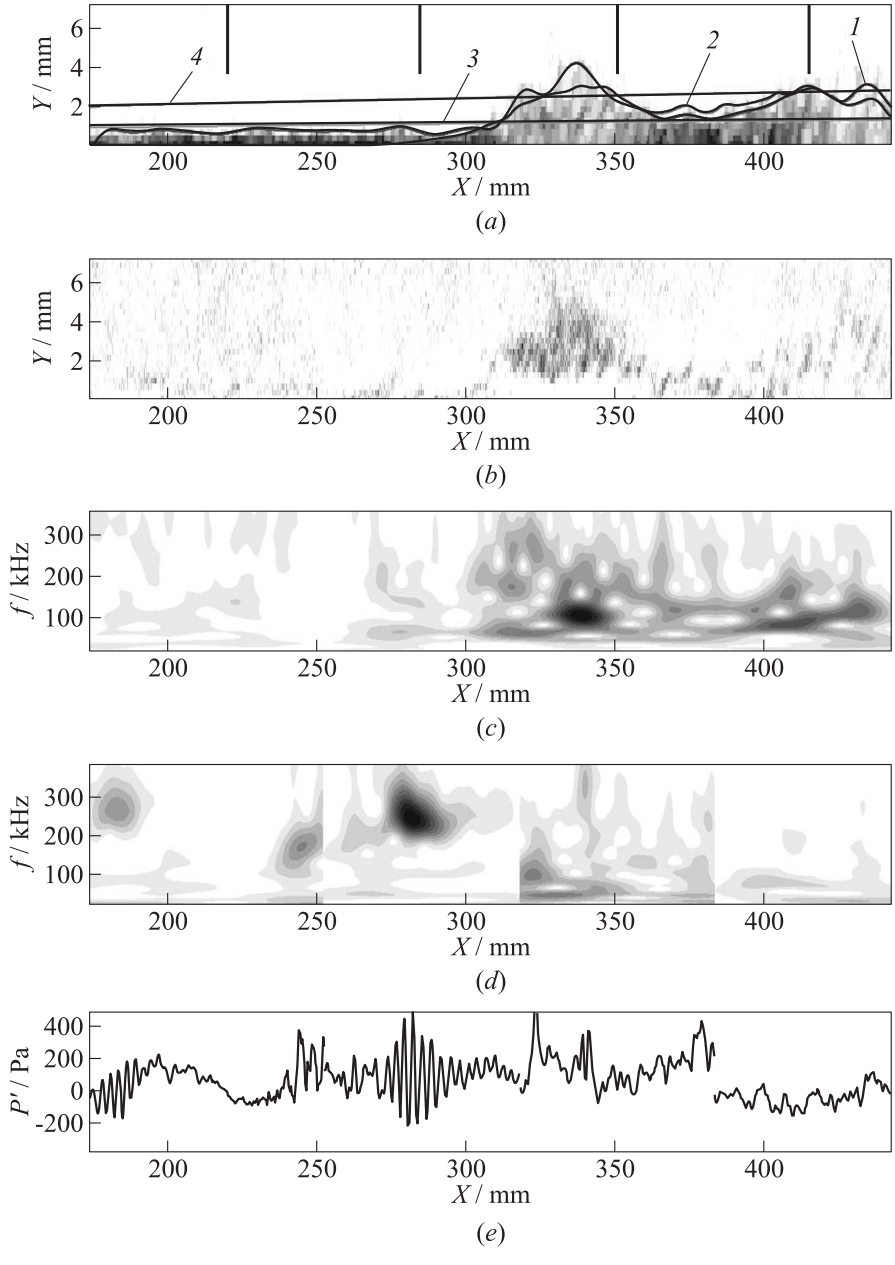

Figure 5 The data processing of schlieren image at $\mathrm{Re}_1 = 8.5 \cdot 10^6$ m^{-1} and $R_n = 0.07$ mm

Fig. 3*b*. The intensity of an image was used to calculate streamwise root mean square (RMS) value shown in Fig. 3*a* by curve *2*. Here, the RMS value is averaged across the boundary layer and multiplied by a scale factor. This factor was defined once and used for processing of all data. It can be seen from the figure that in the turbulent spot, curves *1* and *2* coincide (Figs. 3–5). Finally, it can be concluded that using of RMS level as a criteria allows to minimize the amount of erroneously detected turbulent spots.

The spectral characteristics of the boundary layer structures were obtained by wavelet analysis. The wavelet transform was done using MATLAB software. The Morelet mother wavelet was used [5]. From Figs. 3*b*–5*b*, one can see that the periodical structures in the boundary layer have inclination of the same value. This value was used to calculate the streamwise shift of the rows for calculation of streamwise distribution of intensity fluctuations averaged across the boundary layer. The result of the wavelet analysis of this distribution is shown in Fig. 3*c*. The coordinate transform was used to obtain time scale and pulsation frequency $dt = dx/(0.9U)$ where sx is the pixel size; U is the flow speed above the boundary layer; and the constant 0.9 was obtained from travel speed of the turbulent spots.

To compare the pressure pulsation data and data of the schlieren visualization, it was assumed that the level of the pressure pulsations is almost constant near the sensor. The black vertical lines in Figure 3 show the positions of the sensors. Using the transformation of coordinates $x = x_{\text{sens}} - (t - t_0) \cdot 0.9U$ (where $x_{\text{sens}}$is the coordinate of the sensor and t_0 is the frame time), it is possible to calculate an instantaneous distribution of pressure along the model (see Fig. 3*e*). There are some discontinuities of the pressure distribution obtained in such a manner. These discontinuities are important only for high frequencies; therefore, such instantaneous pressure distributions may be used for qualitative analysis. The result of wavelet transform of the pressure distribution is presented in Fig. 3*d*.

2.2 Experimental Results

The present paper presents the experimental data and corresponding analysis for 3 experiments performed for the following conditions: $\text{Re}_1 = 8.5 \cdot 10^6$ (R_n = 0.07 mm); $12.5 \cdot 10^6$ (R_n = 0.75 mm); and $33.1 \cdot 10^6$ m^{-1} (R_n = 0.75 mm). Figure 6 shows the intermittency distributions calculated for these three runs as ratio of number of frames where the turbulent spot was detected at a particular x to the total number of frames. It can be seen that increase of the nose bluntness results in delay of laminar–turbulent transition.

Due to limited camera resolution, the thickness of the laminar boundary layer is only 3–5 pixel. This is not enough to resolve the fluctuations of the density gradient corresponding to the second mode in the laminar boundary layer. Therefore, all fluctuations of intensity in the schlieren images and wavelet plots

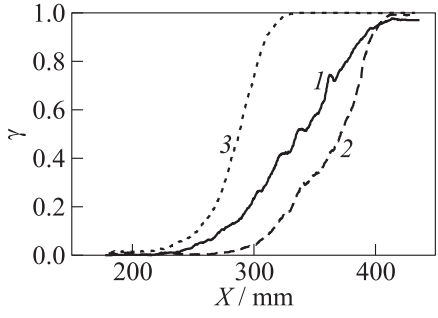

Figure 6 Intermittency in the transitional boundary layer: *1* — $R = 0$ mm and $\mathrm{Re}_1 = 8.5 \cdot 10^6$ m^{-1}; *2* — $R = 0.75$ mm and $\mathrm{Re}_1 = 12.5 \cdot 10^6$ m^{-1}; and *3* — $R = 0.75$ mm and $\mathrm{Re}_1 = 33.1 \cdot 10^6$ m^{-1}

are the result of the density gradient pulsations in the turbulent spots.

Figures 3 and 4 show two consequent frames obtained with delay of 0.085 ms (corresponding to travel distance of 62.55 mm) for $\mathrm{Re}_1 = 8.5 \cdot 10^6$ m^{-1} and $R_n = 0.07$ mm. From Fig. 3, one can see one incipient turbulent spot ($x = 220$ mm) and one well developed ($x = 280$ mm) with pulsations corresponding to the second mode (250–350 kHz). Intensity fluctuations for the second turbulent spot are more pronounced. From Fig. 4, one can see that the size of the first turbulent spot does not change significantly ($x = 280$–300 mm), the pulsations corresponding to the second mode are dumped, and low frequency pulsations are more pronounced. The second turbulent spot significantly grows ($x = 330$–350 mm) and pulsations of the second mode are also dumped. These two figures prove the fact that the coherent structures in the turbulent spot at its initial stage are connected with the second mode. In the process of the spot development, the mark of the second mode diminishes. The amplitude of the second mode pulsations cannot be considered as a criteria of the beginning of the turbulent spot formation. For example, in Fig. 5, there are powerful fluctuations of intensity at $x = 280$ mm but there is no inflation of the boundary layer thickness; so, the turbulent spot is not detected here.

It can be assumed that in the wind tunnel experiment, development of the second mode is not the only one mechanism of the turbulent spot origination. It is rather possible that low-frequency pulsations are able to develop to a turbulent spot. Moreover, from the wavelet amplitude in Figs. 3–5, one can see that there are some peaks at low frequency corresponding to coordinates of the incipient turbulent spots. These peaks are associated with coherent structures in the boundary layer which transforms to a turbulent spot downstream.

Using the pressure pulsation amplitude as a criterion of the turbulent spot beginning is also under investigation. It is necessary to take into account that surface pressure pulsations produced by the first mode and vortices of the turbulent boundary layer are significantly lower than pressure pulsation for the second-mode even if the energy of disturbances is the same.

Figure 7 presents variation of the intermittency during a run (averaging windows 2.5 ms). It is clearly seen that the position of the laminar–turbulent transition slightly changes. It was decided to use the thickness of the boundary

layer as a parameter for definition of the boundary layer state in a particular position. Based on this criterion, all pressure pulsation spectra may be divided into several groups and averaged. The thickness of laminar boundary layer $\delta_{\text{lam}}(x)$ was calculated based on Blasius solution (shown by curves *3* in Figs. 3–5). After that, all data were divided into 4 groups: (*i*) $\delta \le \delta_{\text{lam}}(x)$ (lam.); (*ii*) $\delta_{\text{lam}}(x) < \delta \le 1.4\delta_{\text{lam}}(x)$ (turb. #1); (*iii*) $1.4\delta_{\text{lam}}(x) < \delta \le 1.8\delta_{\text{lam}}(x)$ (turb. #2); and (*iν*) $1.8\delta_{\text{lam}}(x) < \delta$ (turb. #3, curves *4* in Figs. 3–5). The number of samples depending on the position of sensor and the state of the boundary layer is shown in Fig. 8.

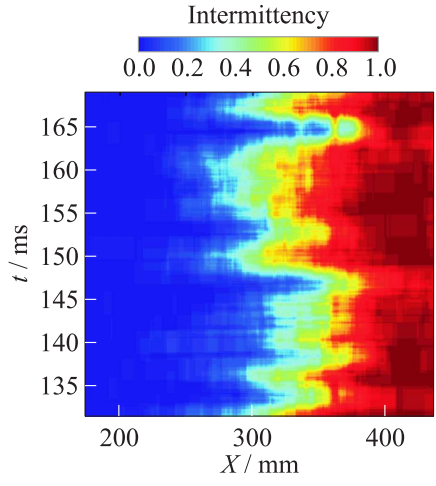

Figure 7 Intermittency during the run at $\text{Re}_1 = 8.5 \cdot 10^6$ m^{-1} and $R_n = 0.07$ mm

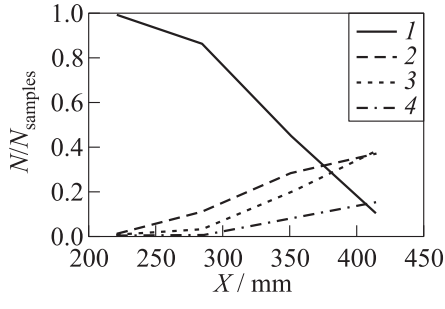

Figure 8 Number of samples used for calculation of the spectrum (*1* — lam.; *2* — turb. #1; *3* — turb. #2; and *4* — turb. #3) at $\text{Re}_1 = 8.5 \cdot 10^6$ m^{-1} and $R_n = 0.07$ mm

The spectra of pressure pulsations for every boundary layer state are presented in Fig. 9. At the second and third sensors (Figs. 9*a* and 9*b*), there is a slight change of the spectra depending on the state of the boundary layer. These sensors are located at the beginning of the zone of laminar–turbulent transition and structures in the turbulent spot connected with the second mode perturbations. The spectrum for the state turb. #3 in Fig. 9*a* is probably a result of low statistics. In Fig. 9*c*, there are clearly visible differences between the spectra. Decrease of the second mode amplitude and growth of the low-frequency disturbances occurs with an increase of the turbulent spots thickness. At the fifth sensor, the difference between the spectra is negligible, but the peak pulsation of the second mode can still be found for the laminar state of the boundary layer. These data show that thickness of the boundary layer is not a good criterion for definition of the turbulent spot evolution stage. Most probably, more information can be obtained if the pulsation level of the intensity of Schlieren image will be used for this purpose.

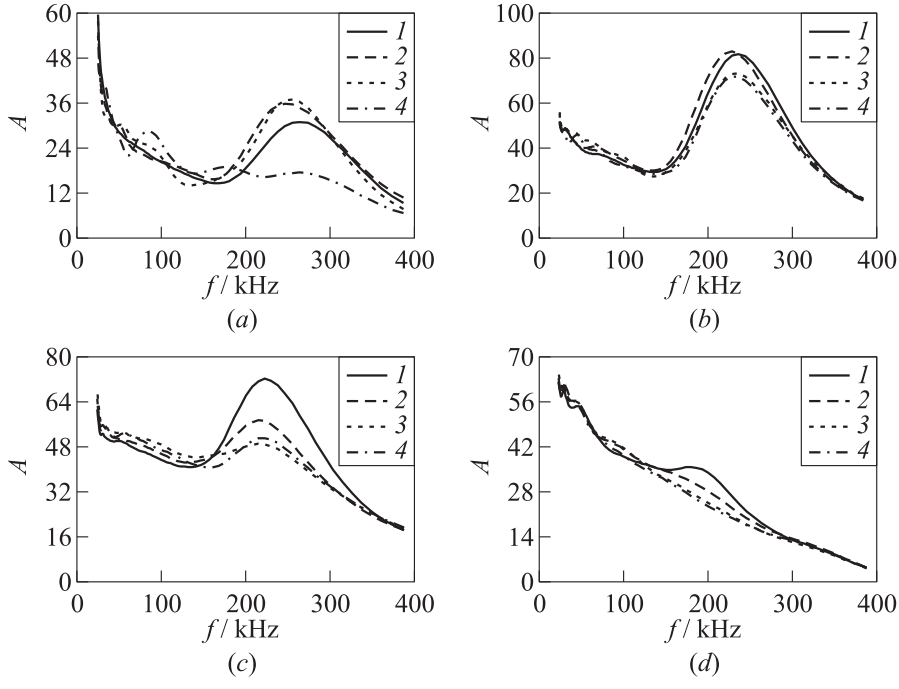

Figure 9 Spectra of the wall pressure pulsations depending on the state of the boundary layer at 218.6 (*a*), 283.6 (*b*), 348.6 (*c*), and 413.6 mm (*d*) ($\mathrm{Re}_1 = 8.5 \cdot 10^6$ m^{-1} and $R_n = 0.07$ mm): *1* — lam.; *2* — turb. #1; *3* — turb. #2; and *4* — turb. #3

To improve the analysis, it was decided to consider the evolution of individual turbulent spots. Because it is difficult to detect the individual turbulent spots at the end of the laminar–turbulent transition region, it was decided to take into account only the spots that arise at the beginning of the measurement zone. In Fig. 10*a*, one can see an example of development of a single turbulent spot. Calculation of the spectra was carried out by averaging the wavelet data within the investigated turbulent spot. The resulting contours of the amplitude of spectra vs. position of the spot are shown in Figs. 9*b* and 9*c*. The average thickness of the turbulent spots are shown on the right side of the figures. It is clearly seen that at the beginning of the turbulent spot, the peak of pressure pulsations can be found at the frequency of the second mode. During the growth of the turbulent spot, the low-frequency pulsations of wall pressure are increased and high-frequency component is decreased. The pulsations of the intensity of schlieren image are qualitatively similar to the data of pressure sensors, but high-frequency perturbations are omitted.

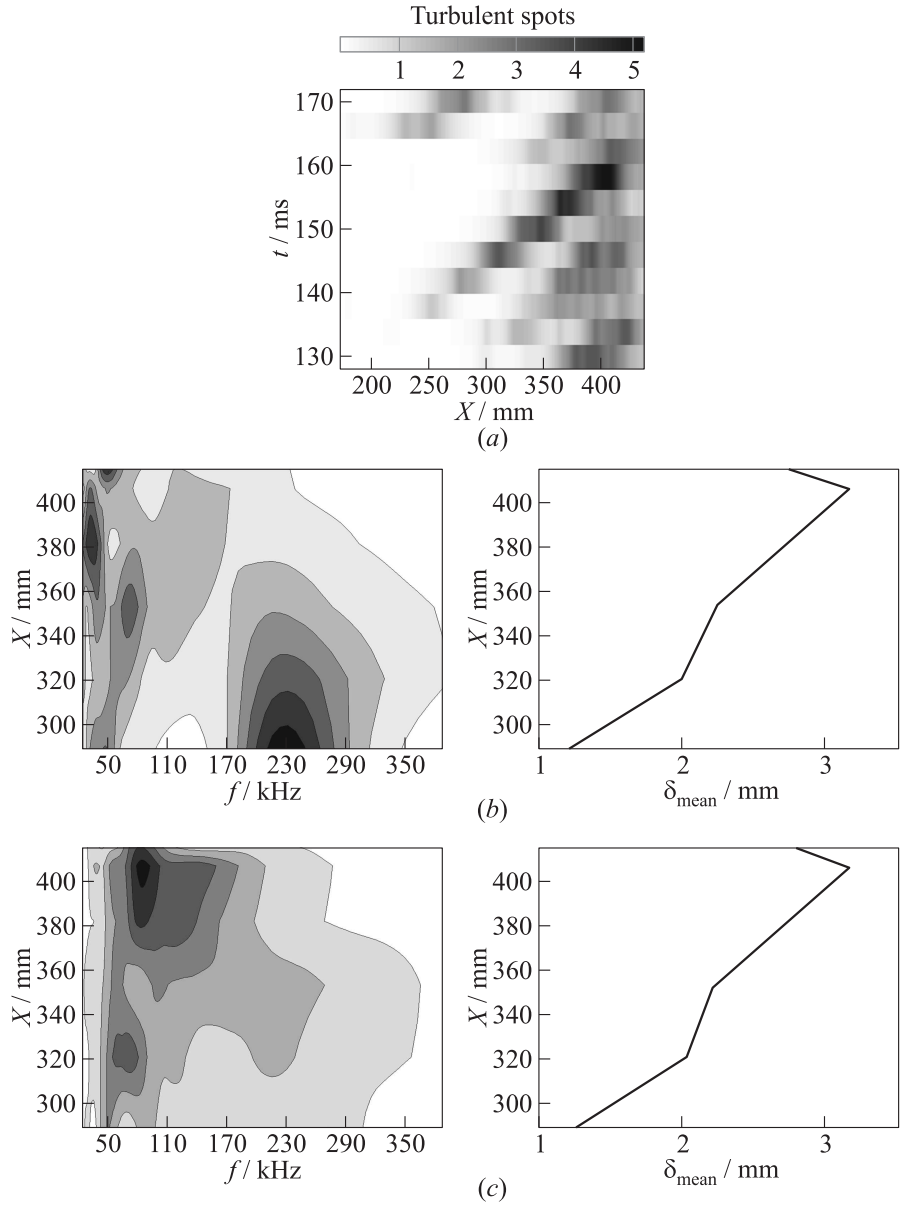

Figure 10 Evolution of turbulent spots (a); wall pressure pulsations (b); and pulsations of image intensity (c) at $\mathrm{Re}_1 = 8.5 \cdot 10^6$ m^{-1} and $R_n = 0.07$ mm

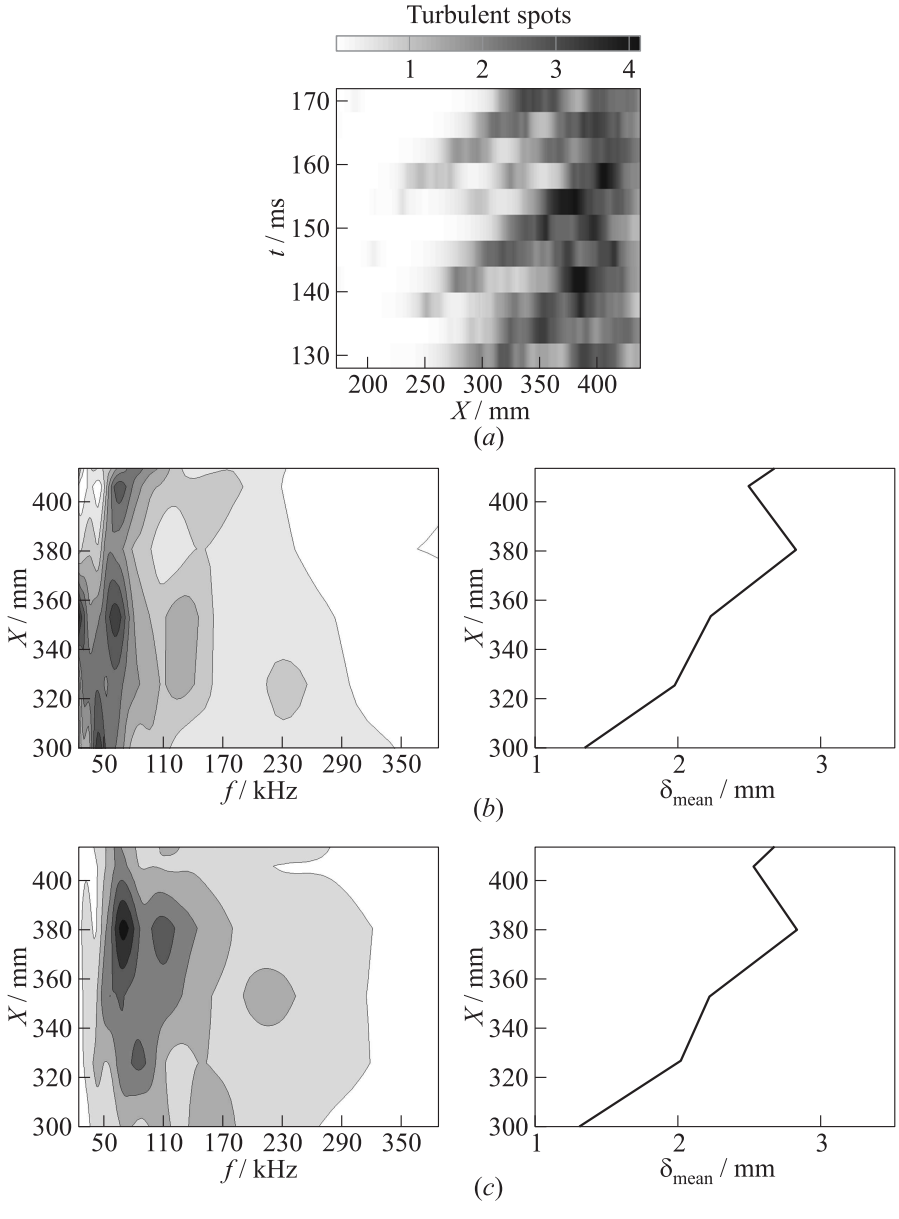

Figure 11 Evolution of turbulent spots (a); wall pressure pulsation (b); and pulsation of image intensity (c) at $\mathrm{Re}_1 = 8.5 \cdot 10^6$ m^{-1} and $R_n = 0.07$ mm

The most part of the data ($> 80\%$) was obtained for individual turbulence spots similar to the results of Fig. 10. One can assume that in this paper, the main cause of the laminar–turbulent transition is the development of the disturbances of the second mode. But part of the data shows that in the process of the turbulent spot development, the level of high-frequency pulsations is negligible (Fig. 11). It is interesting to note that in the process of development of the turbulent spots, there is no significant increase of pressure pulsations on the wall but the increase of the level of pulsation in the schlieren image (see Fig. 11*c*) is evident. This means that the level of wall pressure pulsation not always can be used for the analysis of the state of the turbulent spots.

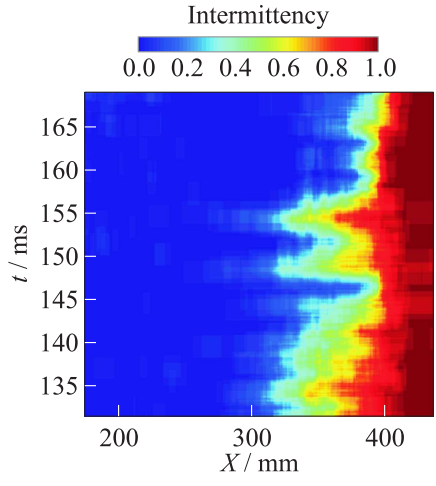

Figure 12 Intermittency during the run at $\mathrm{Re}_1 = 12.5 \cdot 10^6$ m^{-1} and $R_n = 0.75$ mm

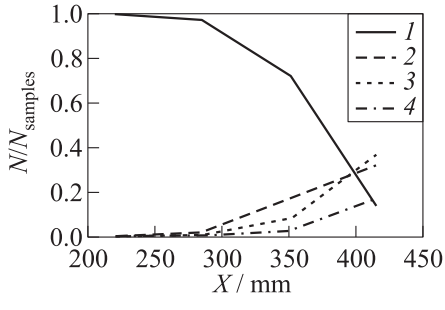

Figure 13 Number of samples used for calculation of the spectrum (*1* — lam.; *2* — turb. #1; *3* — turb. #2; and *4* — turb. #3) at $\mathrm{Re}_1 = 12.5 \cdot 10^6$ m^{-1}and $R_n = 0.75$ mm

Figures 12 and 13 show the results obtained for $\mathrm{Re}_1 = 12.5 \cdot 10^6$ m^{-1} and $R_n = 0.75$ mm. It can be noted that in comparison with the previous data, in this case, the laminar–turbulent transition is shorter. For this experiment, it is possible to achieve a better division of the pulsation spectra into the groups corresponding to different states of the boundary layer. At the second sensor (Fig. 14*a*) the growth of the second mode with increasing thickness of the turbulent spot takes place. The low value of the amplitude of the second mode for the laminar regime can be explained by low duty cycle of the wave packets of the second mode. At the third sensor (Fig. 14*b*) increasing thickness of the turbulent spots is attended by growth of the low-frequency wall pressure pulsation. The second mode pulsations are growing at the beginning of the turbulent spots, but further development of the spot leads to their decay. The results for sensors 4 and 5 are qualitatively similar to the data obtained for the third sensor.

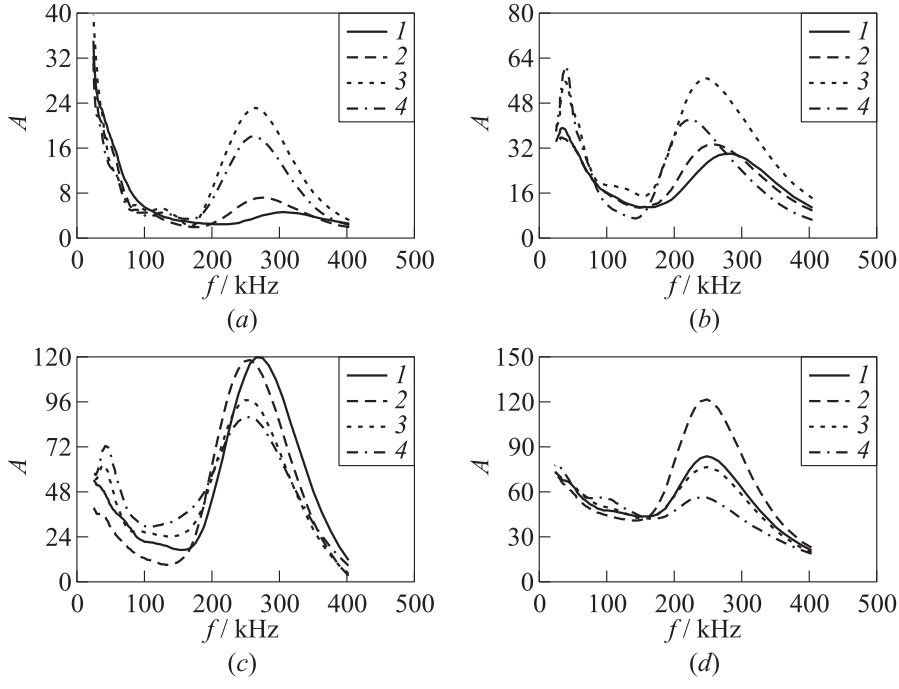

Figure 14 Spectra of the wall pressure pulsations depending on the state of the boundary layer at 218.6 (*a*), 283.6 (*b*), 348.6 (*c*), and 413.6 mm (*d*) ($\mathrm{Re}_1 = 12.5 \cdot 10^6$ m^{-1} and $R_n = 0.75$ mm): *1* — lam.; *2* — turb. #1; *3* — turb. #2; and *4* — turb. #3

A possible reason of better separation of the spectra presented in Fig. 14 compared with the spectra of Fig. 9 is the difference in the turbulent spot evolutions. It seems that in the case of blunted nose, the role of the second mode in the origination of the turbulent spot is dominant. This is confirmed by the analysis of the development of individual turbulent spots. In contrast to the sharp nose case, all the data are qualitatively similar and show that mainly at the beginning of a turbulent spot, there are pulsations at the frequency of the second mode. The parameters of single turbulent spot evolution for the case of $\mathrm{Re}_1 = 12.5 \cdot 10^6$ m^{-1} and $R_n = 0.75$ mm are shown in Fig. 15.

3 CONCLUDING REMARKS

In the paper, the combined data processing algorithm for coupling of unsteady pressure sensors with high-speed schlieren images was proposed. It was shown

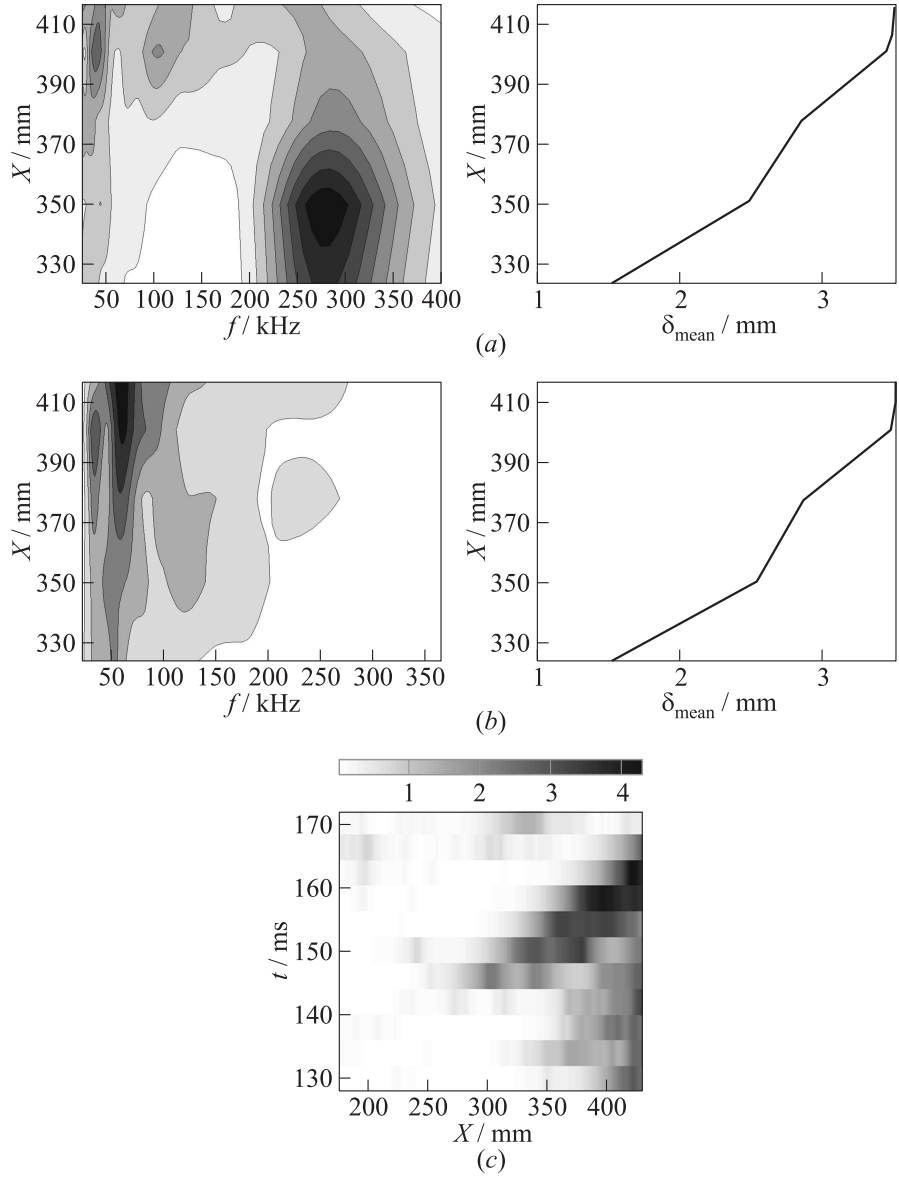

Figure 15 Evolution of turbulent spots (a); wall pressure pulsation (b); and pulsation of image intensity (c) at $\mathrm{Re}_1 = 12.5 \cdot 10^6$ m^{-1} and $R_n = 0.75$ mm

that using of wavelet analysis of schlieren image, it is possible to recognize the typical states of the transitional boundary layer. Analysis of the evolution of individual turbulent spots shows that its characteristic frequency decreases beginning from the second mode frequency to lower value during its development downstream. It was found that for the blunted model, the role of the second mode in origination of the turbulent spot is more evident. The results of this study show that measurement and analysis of nonstationary wall pressure are not sufficient for the study of the laminar–turbulent transition processes.

ACKNOWLEDGMENTS

The work was supported by the Russian Science Foundation (grant No. 14-11-00490p).

REFERENCES

1. Sidorenko, A. A., P. A. Polivanov, Y. V. Gromyko, D. A. Bountin, and A. A. Maslov. 2013. Effect of the local wall cooling/heating on the hypersonic boundary layer stability and transition. *5th European Conference for Aeronautics and Space Sciences (EUCASS)*. Munich, Germany.
2. Casper, K. M., S. J. Beresh, J. F. Henfling, R. W. Spillers, and B. O. M. Pruett. 2014. Toward transition statistics measured on a 7-degree hypersonic cone for turbulent spot modeling. AIAA Paper No. 2014-0427.
3. Zvegintsev, V. I. 1992. Impulse aerodynamic wind tunnel with electric heater. *Conference (International) on the Methods of Aerophysical Research Proceedings*. Novosibirsk, Russia: ITAM SB RAS. II:171–173.
4. Gromyko, Yu. V., V. A. Polivanov, A. A. Sidorenko, D. A. Buntin, and A. A. Maslov. 2013. An experimental study of the natural noise in the Transit-M hypersonic wind tunnel. *Thermophys. Aeromech.* 20(4):481–493.
5. Torrence, C., and G. P. Compo. 1998. A practical guide to wavelet analysis. *Bull. Am. Meteorol. Soc.* 79(1):61–78.